Numerical investigation of the surface recrystallization during the extrusion of a AA6082 aluminum alloy under different process conditions

(Article begins on next page)

09 January 2025

Numerical investigation of the surface recrystallization during the extrusion of a AA6082 aluminum alloy under different process conditions

Marco Negozio[1], Riccardo Pelaccia[2], Lorenzo Donati[1], Barbara Reggiani[2,3]

[1]DIN Department of Industrial Engineering – University of Bologna,

Viale Risorgimento 2, 40136, Bologna, Italy.

[2]DISMI Department of Sciences and Methods for Engineering, University of Modena and Reggio Emilia,

Via Amendola 2, 42122, Reggio Emilia, Italy.

[3]InterMech - MO.RE – University of Modena and Reggio Emilia, Piazzale Europa 1, Reggio Emilia 42124, Italy

CORRESPONDING AUTHOR:

Marco Negozio

DIN Department of Industrial Engineering – University of Bologna

Viale Risorgimento 2, 40136, Bologna, Italy.

tel: +39 051 2090 496

e-mail: marco.negozio2@unibo.it

Abstract

The microstructure of 6xxx aluminum alloys deeply affects mechanical, crash, corrosion and aesthetic properties of extruded profiles. Companies, especially in the transportation sector, require control over the grain structure in order to ensure the quality and the performance of the products. A main challenge for the extrusion companies is to accurately predict the profile microstructure at the design stage, trying to limit the formation of coarse grains and, consequently, the reduction of the mechanical properties of the component. In this work, the modeling of the stored energy, driving force for the recrystallization, was carried out and implemented within the Qform Extrusion FEM code. A novel approach for the evaluation of fibrous and recrystallized microstructures in 6XXX aluminum alloy profiles was proposed and tested in a campaign of experiments involving the extrusion of AA6082 round bars under several die designs and processing conditions. The outcomes proved the good accuracy of the recrystallization predictions during the extrusion of AA6082 aluminum alloy.

Keywords: microstructure, recrystallization, finite element analysis, simulation, aluminum alloys, stored energy, Zener Drag pressure

Article Highlights

- Simulation by means of FEM codes of the extrusion process of 6XXX aluminum alloys
- Developing an analytical model for the stored energy prediction during the extrusion process of 6XXX aluminum alloy
- Numerical assessment of the recrystallized thickness of 6XXX extruded profile

Introduction

The microstructure of aluminum alloys significantly affects mechanical, aesthetic, corrosion and crash properties [1-5]. Especially in the transportation field (i.e. aeronautical, automotive, railway, etc), requirements in terms of grain structure have to be respected in order to ensure the quality of the product. According to those standards, the fibrous microstructure is often preferred to the recrystallized one since it optimizes the mechanical resistance and the energy absorption properties of the components [6]. Unfortunately, the grain structure evolution during hot forming processes is a complex phenomenon because several parameters such as alloy chemical composition, temperatures, extrusion speed, tools geometries, quenching and thermal treatment properties deeply affect the recrystallization behaviour of aluminum alloys. To date, the recrystallization kinetics are not fully understood and, consequently, investigations are needed to evaluate the influence of the process and material parameters on the microstructure evolution for critical aluminum alloys.

In Fig. 1, a typical microstructure evolution during the extrusion of aluminum alloys is shown. In the fibrous structure (Fig. 1b,d), grains are deeply elongated and characterized by the dimension along the extrusion direction several times greater than the width and thickness. Instead, in the recrystallized structure (Fig. 1c,e), grains restore partially or totally their initial equiaxed state (Fig. 1a) characterized by a single average grain diameter. The fully recrystallized state is always detectable in the billet material as a consequence of the casting phase and further homogenization process. Immediately after the die exit, the profile always shows a fibrous microstructure (immediate profile quenching) due to the strain field applied in the extrusion process. If the profile is not immediately quenched or exposed to an annealing treatment, the structure may recrystallize (fully or partially as shown in Fig. 1c,e). It also may remain fibrous, if the energy stored in the material during the deformation process is lower than a certain critical level (Fig. 1d).
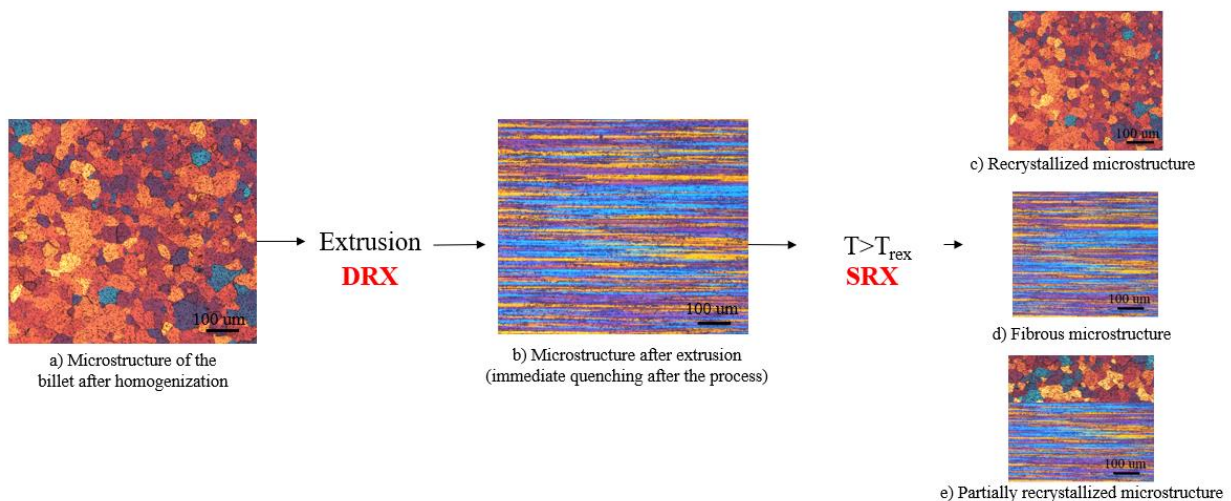
Fig. 1: Schematic microstructure evolution during extrusion (extrusion direction from sx to dx).

In the extrusion processing, two main recrystallization mechanisms can be distinguished: the first, called dynamic recrystallization (DRX), occurs in the billet during material deformation while the second, called static recrystallization (SRX), occurs in the extruded profile, after the deformation [7]. DRX is related to the material strain field and produces, in low stacking fault materials (LSFE as steels), nucleation and grain growth or, in high stacking fault materials (HSFE as aluminum alloys), different phenomena which have been heavily debated by the scientific community. Several studies have been made to investigate the DRX mechanism in aluminum alloys. In 2003, Goudet S and

Montheillet F [8] theorized that, during the deformation, new grains are generated by the change of the misorientation angle of subgrains LAGB (Low Angle Grain Boundaries) becoming HAGB (High Angle Grain Boundaries) thus generating a new grain. This theory is called cDRX (Continuous Dynamic Recrystallization). In 2004 and 2011, McQueen HJ et al. [9-10] proposed that, due to the process strain field, the original grains flatten and elongate until the grain thickness becomes in the order of 2-3 times the subgrain size and, as consequence, the grain is pinched-off and two smaller grains are generated. This recrystallization theory is called gDRX (Geomentric Dynamic Recrystallization). In 2008, De Pari L and Misiolek W [11] proposed to consider both effects theorizing a joint model called jDRX (Joint Dynamic Recrystallization) successfully verified on a AA6061 during the hot rolling process. This model was also investigated by Donati L et al. [12] in 2013.

The second main recrystallization mechanism is the static recrystallization (SRX), which occurs after the hot deformation and causes the rearrangement of the microstructure through nucleation and growth [13]. Several studies have been made to investigate the SRX in the hot deformation processes of aluminum alloys using Finite Element Model (FEM) simulations [14-20]. This phenomenon occurs if the profile has particular energy conditions after the deformation process. These energy conditions involve the stored Energy (Pd) and the Zener Drag pressure (Pz). The stored energy is the driving force for recrystallization and it is accumulated in the form of dislocation and high concentrations of vacancies [21] during the deformation. The Zener Drag pressure acts in opposition to the stored energy [18] and depends on the material temperature, dispersoids distribution and size [22]. Dispersoids are generated during homogenization treatment in relation to the alloying elements content and the homogenization parameters [23-25]. Consequently, the prediction of these two energy components is required in order to simulate and foresee the process conditions that lead to the recrystallization of the extruded profile. Localized recrystallization on the surface in the extruded profiles is known as Peripheral Coarse Grain (PCG) and is a common extruded defect that usually occurs during the extrusion of medium-strength aluminum alloys such as AA6082. This layer affects mechanical, crash, corrosion, fracture and surface quality properties of the profile thus precluding their applicability in the automotive sector [26-28].

Several studies have been carried out on the FEM simulation of the extrusion of aluminum alloys and on the optimization of the process parameters [29-35], but none of these investigated the predictability of the surface recrystallization in medium strength alloys through an extensive numerical-experimental comparison. To the best of the authors knowledge, there are no tools capable of predicting surface recrystallization, fibrous and recrystallized microstructures using FEM simulations. Since the recrystallized thickness deeply affects several properties of the profile, the developing of a numerical model for the surface recrystallization prediction would be of great interest for the industrial sector, allowing extruders and die makers to optimize the performances using the FEM simulation during the die design and process planning stage, thus reducing time consuming and expensive experimental analysis.

In this work, the analytical modeling of the stored energy evolution during hot forming processes was developed and discussed in order to determine the recrystallized thickness in the extrusion of a round bar of AA6082 under different processing conditions. The model was implemented in the Qform Extrusion® environment, an ALE (Arbitrarian Lagrangian Eulerian) code which is optimized for the extrusion simulation. The experimental tests have been performed by Parson N et al. [26], in which the microstructures of AA6082 round profile extruded with different bearings geometries, pre-heating temperatures, ram velocities and quenching conditions were analyzed. The final aim of this work was to develop a stored energy evaluation model optimized to work in post-processing within the Qform

Extrusion® FEM code, to apply it in the extrusions of AA6082 aluminum alloy round bars and to compare the numerical results with the experimental microstructures reported in [26]. In addition, the work proposed an innovative approach to determine the surface recrystallization behavior of aluminum alloys extruded profiles using FEM simulations by the modeling of the stored energy and the Zener Drag pressure.

Experimental Procedure

Different die geometries with various bearing lengths, choke lengths and choke angles were tested in the extrusion of round bars with a 25 mm diameter made by AA6082 aluminum alloy (Mg: 0.70 wt%, Si: 1.00 wt%, Fe: 0.17 wt%, Mn: 0.5wt%) and the data of the microstructures were collected and discussed. In Fig. 2, images of the dies together with data of the bearings geometries (Tab. 1) are described. For the purpose of this work, the microstructural data of the profiles extruded with the R6 -1.5°, R12 +1°, R25 +0° and R35 +3° dies are considered and then compared with the results of the developed simulations. The experimental campaign consisted of extrusion with two billet pre-heating temperatures Tb (350 °C and 500 °C) and four ram speeds (5 mm/s, 20 mm/s, 30 mm/s, 40 mm/s). For the extrusion made at Tb=350 °C, the tools (die, bolster and container) were pre-heated at 330 °C, while, for the extrusions made at Tb=500 °C the tools were heated at 480 °C.
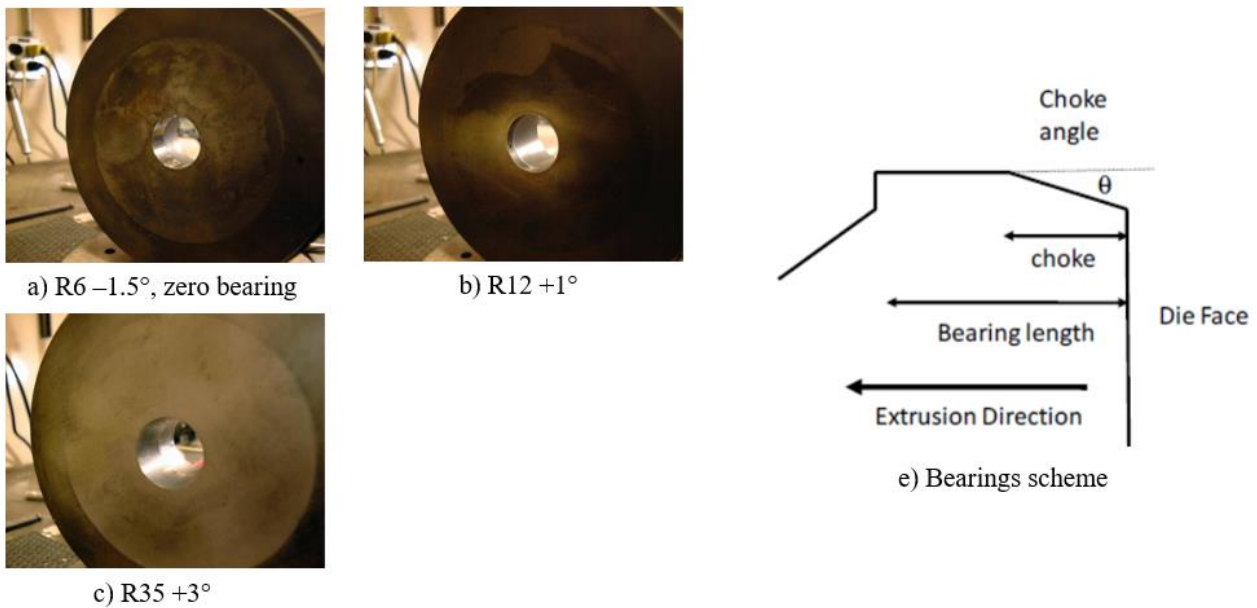

a) R6 −1.5°, zero bearing

b) R12 +1°

c) R35 +3°

e) Bearings scheme

Fig. 2: images and scheme of the die geometries [26]

Table 1: bearings data [26]

ID	Bearing Length [mm]	Choke Length [mm]	Angle deg.
R6 – 1.5°	6	Zero bearings	-1.5
R12 +1°	12	6	+1
R25 +0°	25	Flat	0
R35 +3°	35	17.5	+3

In Fig. 3 and Fig. 4, all the microstructures of the different extruded profiles are reported both in the press-quenched condition (without any solution treatment) and after the solution treatment (30 min at 540°C using a salt bath). Specimens were taken at the middle of the length of the extruded profiles. The x-axis reports the type of bearing geometry tested during the extrusion while the y-axis the ram

speed. As it can be seen from the pictures, all the profiles extruded with T_b=350 °C and press-quenching (Fig. 3a) present a fibrous microstructure. The profiles extruded with T_b=500 °C and press-quenching (Fig. 3b) are also fibrous except for T_b=500 °C with dies R6 -1.5° and R25 +0° at higher speeds (over 20 mm/sec), where a surface recrystallized layer (PCG) is visible. For the extrusion made at a pre-heating temperature of 350 °C, the solution treatment greatly affected the static recrystallization behaviour. All of the specimens' microstructures changed from fibrous (Fig. 3a) to partially or fully recrystallized (Fig. 4a). For the extrusions made at a pre-heating temperature of 500 °C, the situation is completely different. In this case, the experimental evidence shows that the solution treatment did not affect the recrystallization of the specimens, as there is no difference in terms of microstructure between Fig. 3b and Fig. 4b.
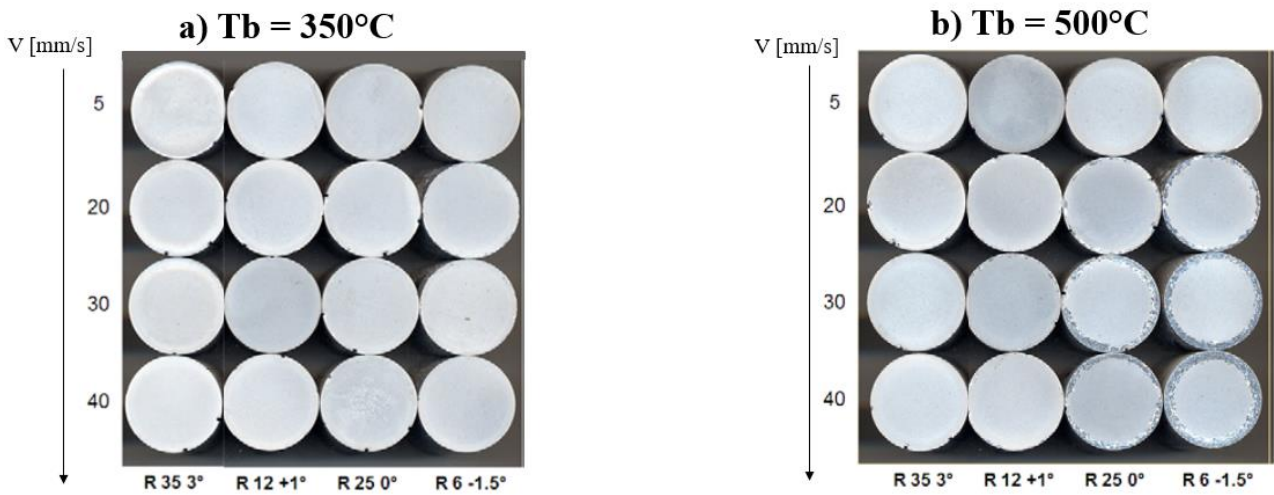

Fig. 3: microstructures of the press quenched specimens [26].

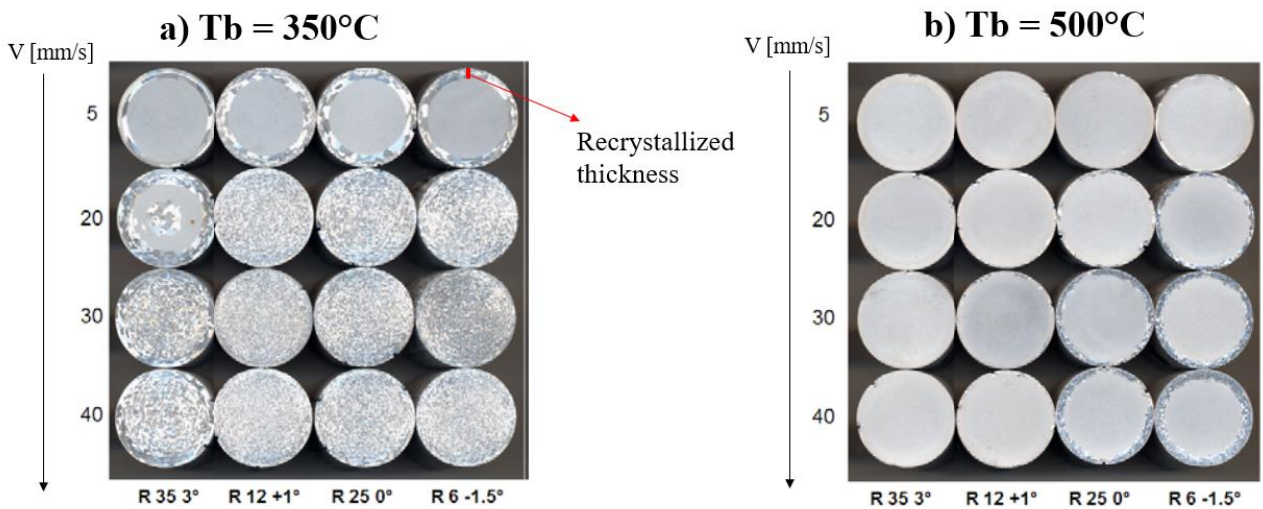**Fig. 4:** microstructures of the solution treated specimens [26].

Numerical Modeling

Analytical Model

Based on the previous work made by [36], the static recrystallization of a 6XXX aluminum alloy happens when the driving forces for the recrystallization are higher than the retarding forces. The stored energy is the driving force for the recrystallization, and it can be calculated according to [17]:

$$\text{Pd} = \frac{Gb^2}{10}\left[\rho_i(1\text{-}\ln(10b\rho_i^{0,5}))+\frac{2\theta}{b\delta}*\left(1+\ln\left(\frac{\theta c}{\theta}\right)\right)\right] \tag{1}$$

where G is the material shear modulus (2.05×10^{10} Pa), b is the Burgers vector (2.86×10^{-10} m), ρ_i is the dislocation density, δ is the subgrain size, θ is the misorientation angle and θc is the misorientation angle limit (15°).

The calculation of the dislocation density ρ_i and the misorientation angle θ was made according to [37]. In more detail, the dislocation density is a function of the strain ε and the Zener-Hollomon parameter Z (Fig. 5a), while the misorientation is a function of the strain rate $\dot{\varepsilon}$ and the temperature T (Fig. 5b).
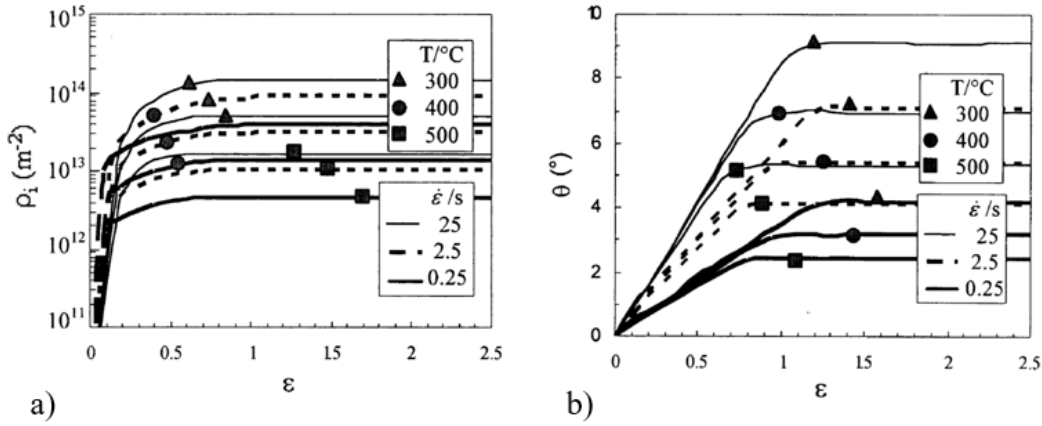

Fig. 5: a) Dislocation density [37]; b) Misorientation angle [37].

The subgrain is evaluated according to [12]:

$$\frac{1}{\delta} = C\,(lnZ)^n \tag{2}$$

where C=3.36×10^{-9} m^{-1} and n=5.577. The Zener-Hollomon parameter is calculated according to [12]:

$$Z = \dot{\varepsilon}\,exp\left(\frac{Q}{RT}\right) \tag{3}$$

where Q is the activation energy of the AA6082 (182000 J/mol*K [38]), $\dot{\varepsilon}$ is the maximum strain rate for each point of material flow during the extrusion deformation path and R is the universal gas constant (8.341 J/mol).

The Zener Drag pressure depends on the dispersoids properties and act in opposition to the recrystallization [23]. It can be expressed as follow:

$$Pz = \frac{3*f*\gamma}{4*r} \tag{4}$$

where f and r are the fraction and the mean size of the dispersoids, respectively, and γ is the grain boundary energy. Since the microstructural data for the f and r evaluation were not available, the values of Pz have been supposed based on the comparison between stored energy and recrystallized thickness of the extrusions made under different process conditions, as explained in more detail in the Result and Discussion section.

7

The stored energy analytical model (Eq. 1-3) was implemented within the Qform Extrusion software using post-processing subroutine feature, which is an interface to calculate user-defined quantities and variables otherwise not considered in the software. In detail, the FEM simulation calculates the values of strain, strain rate and temperature. These values are used for the post-processing analysis as input data for the calculation of the Zener-Hollomon value, the misorientation angle and the dislocation density. Finally, these three variables are further used to calculate the stored energy, which is the only parameter used for the discussion of the results presented in the following chapters.

Numerical Investigation

The numerical simulation of the extrusions was carried out using the Arbitrarian Lagrangian Eulerian FEM code Qform Extrusion®. The simulations were prepared following guidelines obtained by previous validation studies involving the comparison between extrusion simulation outputs as profile exit temperature, material flow and extrusion load to data experimentally acquired [39-42].

As constitutive model for the AA6082 aluminum alloy, the following Hensel-Spittel equation was selected to calculate the material flow stress $\bar{\sigma}$ which depends on the contribution of strain $\bar{\varepsilon}$, strain rate $\dot{\bar{\varepsilon}}$ and temperature T [43]:

$$\bar{\sigma} = A \cdot e^{m_1 T} \cdot \bar{\varepsilon}^{-m_2} \cdot \dot{\bar{\varepsilon}}^{-m_3} \cdot e^{\frac{m_4}{\bar{\varepsilon}}} \cdot (1 + \bar{\varepsilon})^{m_5 T} \cdot e^{m_7 \bar{\varepsilon}} \cdot \dot{\bar{\varepsilon}}^{m_8 T} \cdot T^{m_9} \tag{5}$$

The values of the material parameters (m_1-m_9) are reported in Tab. 2 according to [44].

Table 2: Hensel-Spittel parameters for the AA6082 aluminum alloy [44].

Material parameters	AA6082
A	270 [MPa]
m_1	-0.0045 [K^{-1}]
m_2	-0.127
m_3	0.13
m_4	-0.016
m_5	0.00026 [K^{-1}]
m_7	0
m_8	0 [K^{-1}]
m_9	0

The workpiece-tools friction conditions were set to the default values proposed by the Qform Extrusion database (Tab. 3).

Table 3: Friction conditions.

Surface	Friction condition
Billet-Container	Sticking condition
Billet-Ram	Sticking condition
Billet-Die	Sticking condition
Bearings	Levanov model (m = 0.3, n = 1.25)

The authors also performed an extensive verification of the model numerical accuracy by assessing the effect of the solution parameters on the main output results (stress, strain, temperature fields and extrusion load). A convergence study has been performed by varying the values of the convergence

tolerance (velocities / stress norm) and evaluating the % error in terms of the nodal unknowns. The default values of the minimum norm of velocity increments and stress increments are set to 3% while the performed simulations used a value of 0.5% in order to guarantee a greater level of accuracy.

The extrusions process parameters collected from the experimental campaign and components geometry data are reported in Tab. 4 and Tab. 5.

Table 4: Process parameters.

Process Parameters	
Aluminum alloy	AA6082
Ram speeds [mm/s]	5/20/30/40
Container/Billet/Die temperatures [°C]	380/480
Ram acceleration time [s]	5

Table 5: Extrusion components geometry data.

Extrusion components geometry data	
Extrusion ratio	20
Billet length [mm]	384
Billet diameter [mm]	101
Container diameter [mm]	266
Billet Rest length [mm]	18

The FEM simulation of the investigated extrusion process was validated by the comparison between experimental and numerical breakthrough pressure. In Tab. 6, the experimentally acquired pressures for the 20 mm/s ram speed cases described in [26] are reported and compared to the results of the simulation. The experimental data shows that the R6 -1,5° die gave the lowest value of pressure and, by increasing the bearings length, it increases till the maximum value found using the R35 +3° die. The numerical outputs matched the reported experimental trend, showing errors always below the 5%, thus proving the reliability of the FEM simulations.

Table 6: Comparison between experimental and numerical breakthrough pressures during the extrusions performed with a ram speed of 20 mm/s.

Case study	Experimental breakthrough pressure [MN]	Numerical breakthrough pressure [MN]	Error [%]
R6 -1,5° - Tb=350°C	6,18	6,09	1,46%
R6 -1,5° - Tb=500°C	4,27	4,18	2,11%
R12 +1° - Tb=350°C	6,51	6,44	1,08%
R12 +1° - Tb=500°C	4,55	4,49	1,32%
R25 0° - Tb=350°C	6,83	6,59	3,51%
R25 0° - Tb=500°C	4,82	4,71	2,28%
R35 +3° - Tb=350°C	7,31	6,96	4,79%
R35 +3° - Tb=500°C	5,29	5,04	4,73%

Results and Discussion

Fig. 6 and Fig. 7 report the results of the exit temperatures (highlighted values are taken at the middle profile radius for each specimen) and the stored energy predictions (Eq. 1-3), respectively. The simulation of each case requires an average time of 29 min. In the extrusions made with Tb=350°C, the exit temperatures of the profiles are between 400 °C and 450 °C and the stored energy is significantly higher if compared to the extrusions with Tb=500 °C, where the exit temperatures are between 530 °C and 560 °C. The FEM acquired data are taken at the medium value of the ram stroke because the microstructures reported in Fig. 3 and Fig. 4 were taken from the middle of the extruded profile length.
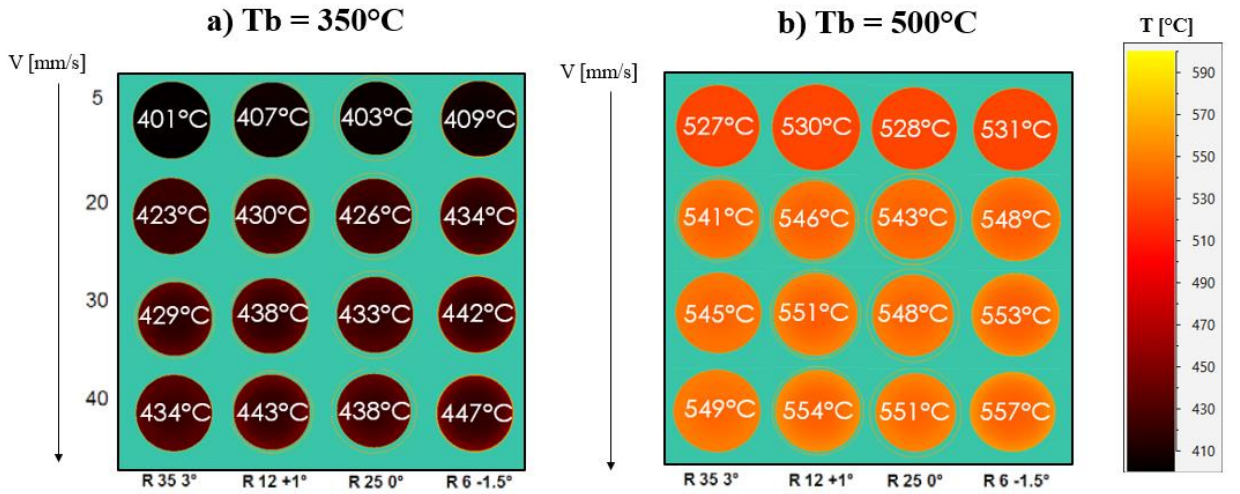

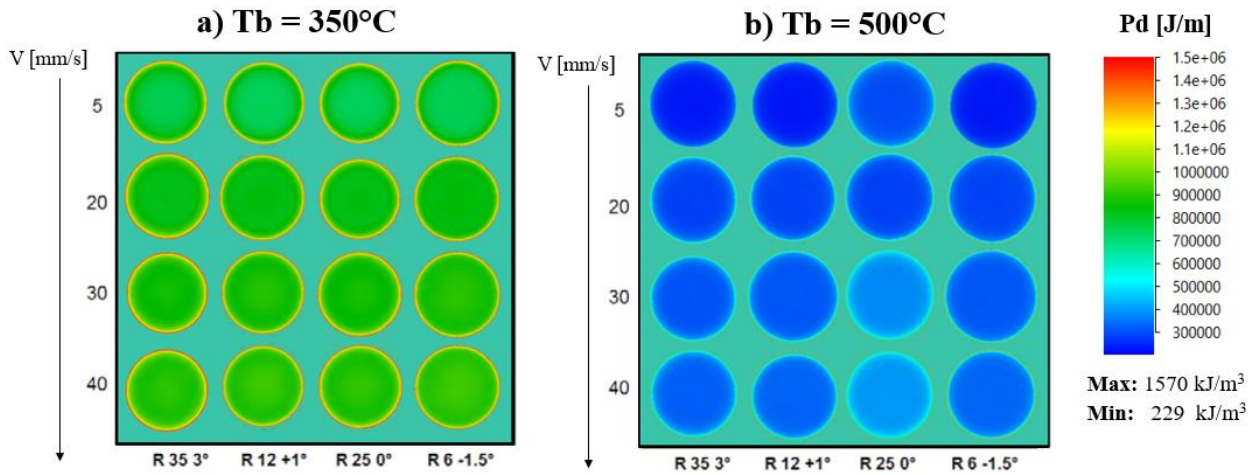**Fig. 6:** Exit temperature.

Fig. 7: Stored energy predictions after extrusion.

The stored energy predictions are then compared with the microstructure for each tested condition in order to understand at what stored energy value the recrystallization occurs. As said, in the specimens extruded with Tb=350 °C in the press-quenched condition, no static recrystallization occurred. Therefore, according to what is reported in the literature [17], the stored energy must always be lower than Pz. For this reason, a Pz value higher than the highest value of Pd found on the simulation is assumed (Pz>1570 kJ/m^3).

In the specimens extruded with Tb=350 °C after the solution treatment, a partially or fully static recrystallization occurred. Consequently, after selecting one extrusion condition for the calibration

(in this case the extrusion made with the R35 +3° die, extrusion speed 5 mm/s, Fig. 8), the value of Pz for the solution treated specimens was taken as the stored energy value in the point where the recrystallized begins (Pz>819 kJ/m^3). The computation of the Pz evaluation process is detailed in Fig. 8 at the radius of 9,5 mm.

In the extrusions made with Tb=500 °C, the microstructure does not change between press quenched and solution treated specimens. For this reason, one single Pz value was assumed for the two conditions (Pz=600 kJ/m^3), using the same methodology applied to the case described before. Different Pz values were adopted for extrusions with different exit temperatures or solution treatment because the Zener Drag pressure is depending on the dispersoids distribution and size which, in turn, depends on the temperature. Consequently, with the purpose to model and predict the recrystallization behaviour, it is reasonable to assume that Pz may change with temperature and, consequently, in particular temperature conditions the SRX is more likely to occur. The validation of this approach and consequently of the assumed values for Zener Drag pressure, will be performed by comparing the recrystallized layer thickness of FEM predictions over experimental data.
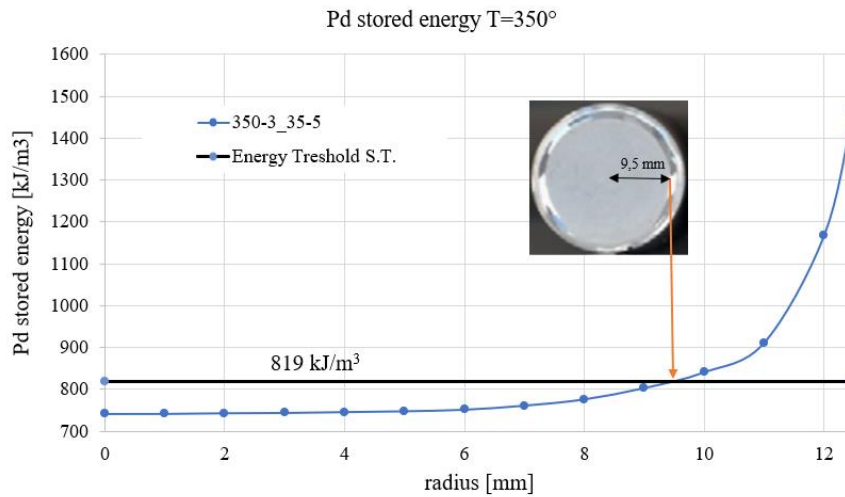

Fig. 8: Zener Drag pressure evaluation process.

Fig. 9 and Fig. 10 show the stored energy behaviour, calculated according to Eq. 1-3, along the specimen radius for the extrusions made with Tb=350 °C (Fig. 9) and Tb=500 °C (Fig. 10). These values were reported together with the supposed Pz values in the press-quenched and solution treated conditions. The general trend of these curves shows a numerical value of stored energy that grows as it approaches the external surface of the profile. Since the strain value grows from the center of the profile to the surface area due to friction and the billet material deformation path, is reasonable to assume that the stored energy will also grow according to the strain.
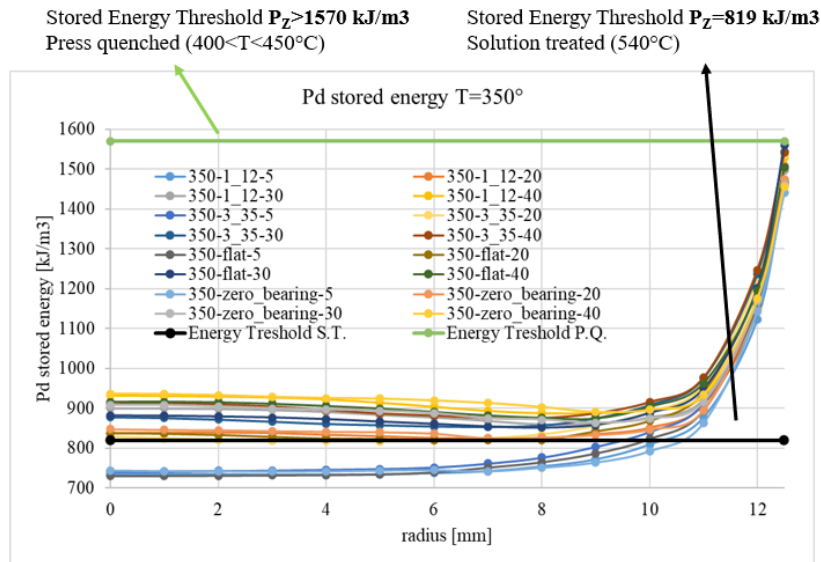
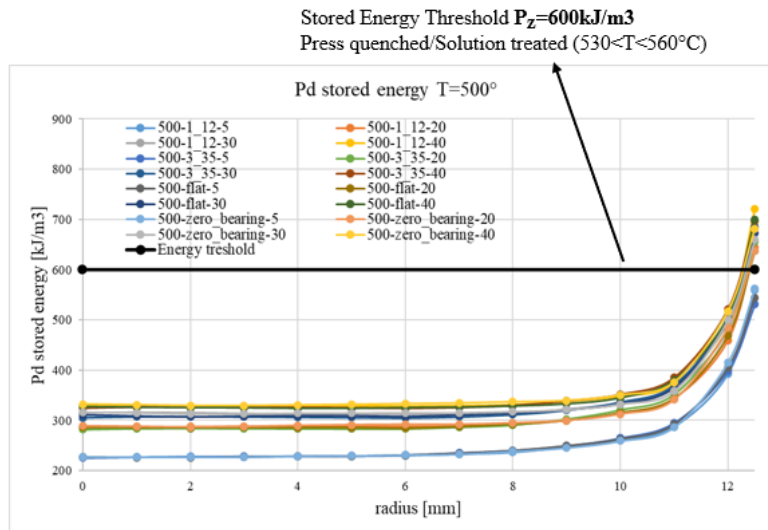**Fig. 9:** Stored energy and stored energy thresholds (Pz values) in the Tb=350 °C case.

Fig. 10: Stored energy and stored energy thresholds (Pz values) in the Tb=500 °C case.

The comparisons between experimental and numerical recrystallized thicknesses are shown in Fig. 11-18 for each bearing geometry and pre-heating billet temperature, in order to validate the methodology and the assumed critical values of Pz. In the left part of each figure, it is shown the stored energy evaluation along the extruded bar radius together with the estimated Pz value. The stored energy values were calculated according to Eq. 1. Two different horizontal lines were reported, one for the stored energy threshold in the press quenched condition and one in the solution treated condition. These lines, obtained as reported in Fig. 9 and 10, cross the stored energy curves thus providing the prediction of the recrystallized thickness for each investigated condition. In the (b) part of the figures, it is reported the comparison between numerical and experimental recrystallized thickness in the press-quenched and solution treated conditions in order to validate the developed model and approach. The first line of the table reports the experimental images of the microstructures. The second line shows the predicted profile recrystallization behaviour in relation to the selected energy threshold: in the press-quenched conditions, if the stored energy is lower than 1570 kJ/m3, the structure remains fibrous (represented in "yellow" in the figure). If, on the contrary, the stored energy is higher than 1570 kJ/m3, the recrystallization occurs, as represented in "green" in the figure.

In the solution treated conditions, if the stored energy is lower than 819 kJ/m3, the structure remains fibrous (represented in "blue" in the figure), otherwise the recrystallization occurs (represented in "red" in the figure). The third line of the table shows the numerical and experimental quantitative comparison between the values of the recrystallized layer thickness. The experimental measures were taken with an accuracy of ±0.2 mm and compared to the relative numerical predictions in Fig. 19.
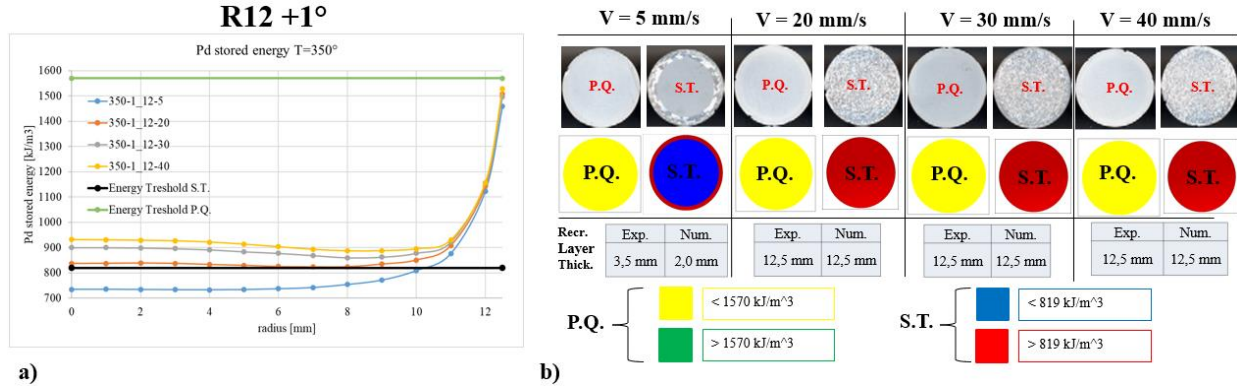

Fig. 11: R12 +1° die, Tb=350°, all speeds. a) stored energy behaviors and comparison with estimated Pz values, b) comparison between numerical and experimental recrystallized thicknesses for Press Quenched (P.Q.) and Solution Treated (S.T.) conditions.
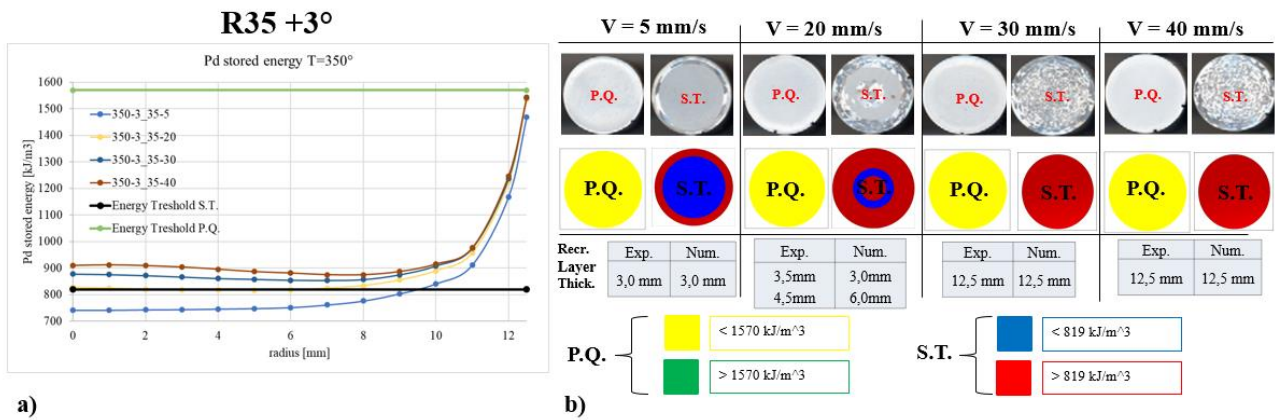

Fig. 12: R35 +3° die, Tb=350°, all speeds. a) stored energy behaviors and comparison with estimated Pz values, b) comparison between numerical and experimental recrystallized thicknesses for Press Quenched (P.Q.) and Solution Treated (S.T.) conditions.
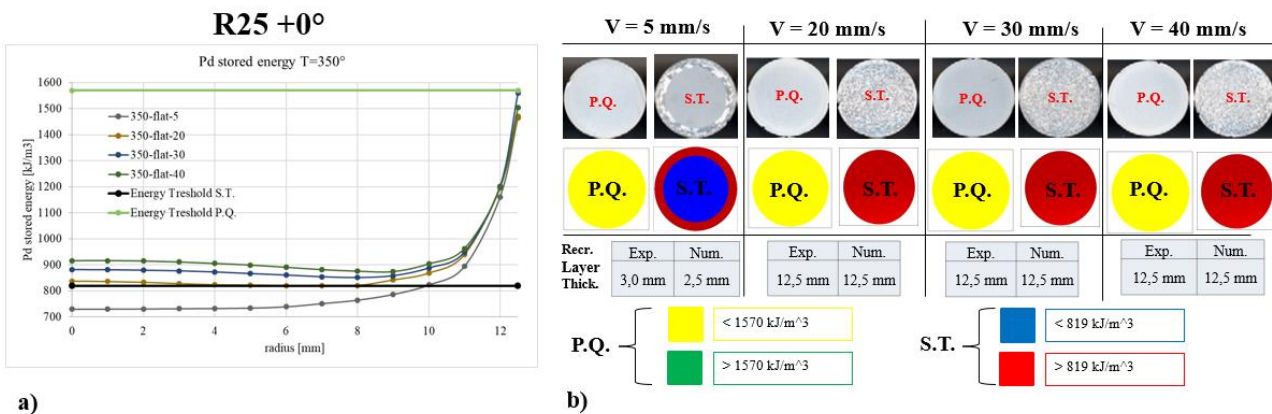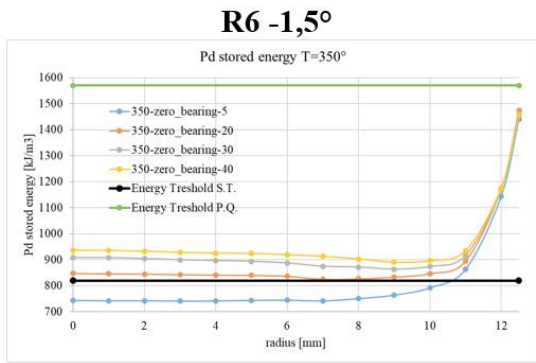

Fig. 13: R25 +0° die, Tb=350°, all speeds. a) stored energy behaviors and comparison with estimated Pz values, b) comparison between numerical and experimental recrystallized thicknesses for Press Quenched (P.Q.) and Solution Treated (S.T.) conditions.
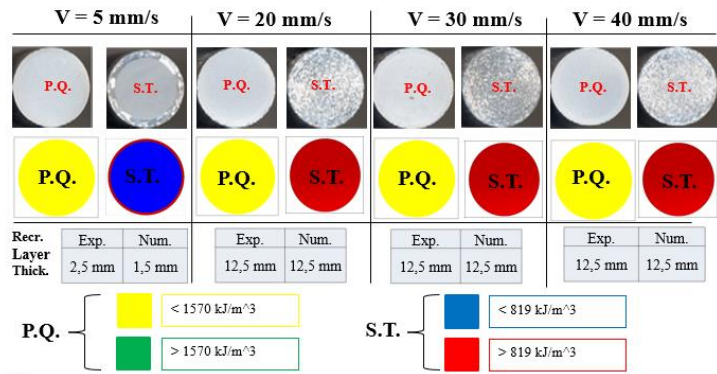
Fig. 14: R6 -1,5° die, Tb=350°, all speeds. a) stored energy behaviors and comparison with estimated Pz values, b) comparison between numerical and experimental recrystallized thicknesses for Press Quenched (P.Q.) and Solution Treated (S.T.) conditions.

Fig. 15: R12 +1° die, Tb=500°, all speeds. a) stored energy behaviors and comparison with estimated Pz values, b) comparison between numerical and experimental recrystallized thicknesses for Press Quenched (P.Q.) and Solution Treated (S.T.) conditions.
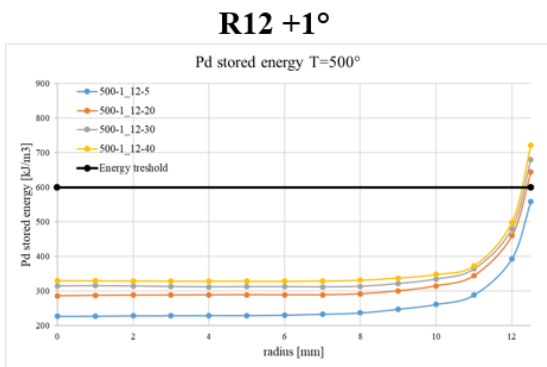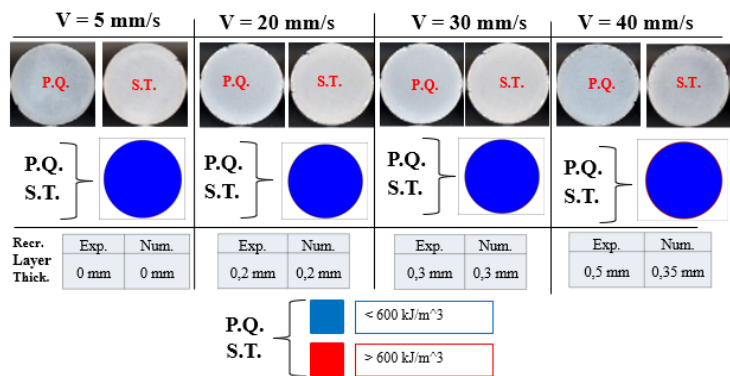

Fig. 16: R35 +3° die, Tb=500°, all speeds. a) stored energy behaviors and comparison with estimated Pz values, b) comparison between numerical and experimental recrystallized thicknesses for Press Quenched (P.Q.) and Solution Treated (S.T.) conditions.

14

Fig. 17: R25 +0° die, Tb=500°, all speeds. a) stored energy behaviors and comparison with estimated Pz values, b) comparison between numerical and experimental recrystallized thicknesses for Press Quenched (P.Q.) and Solution Treated (S.T.) conditions.
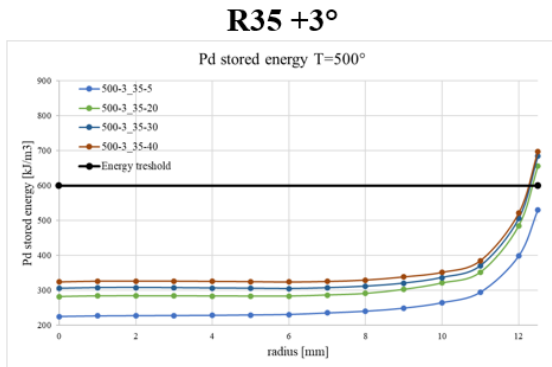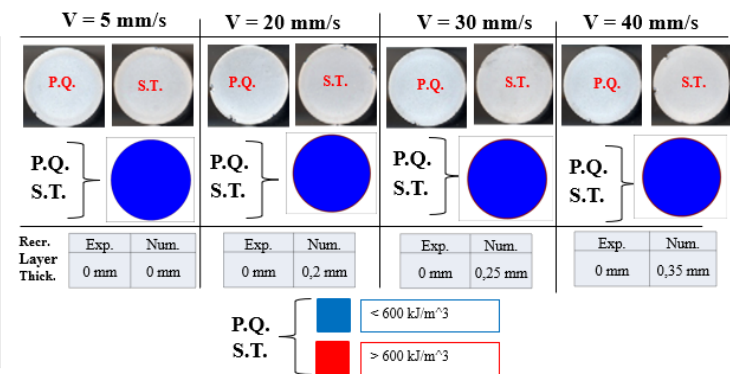

Fig. 18: R6 +1.5° die, Tb=500°, all speeds. a) stored energy behaviors and comparison with estimated Pz values, b) comparison between numerical and experimental recrystallized thicknesses for Press Quenched (P.Q.) and Solution Treated (S.T.) conditions.
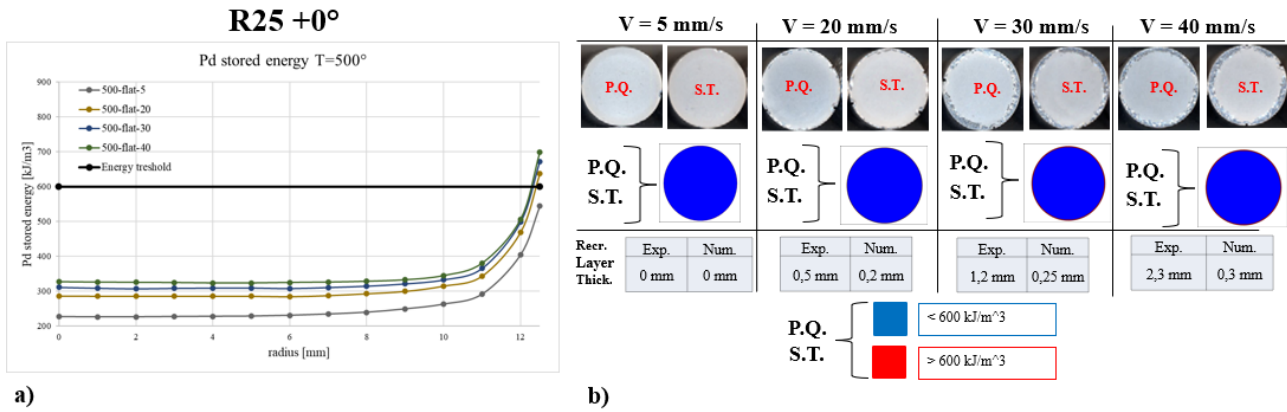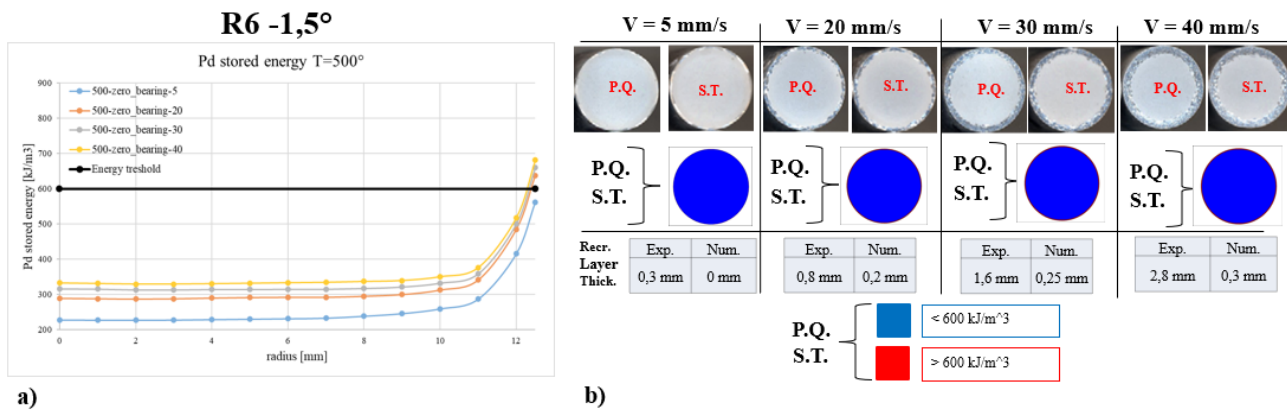
These results show a good model accuracy in the prediction of the recrystallized layers in almost all experimental conditions. The accuracy is higher for the conditions tested with Tb=350 °C. In this case, almost a perfect matching (with a maximum error of 1.5 mm) was found between numerical and experimental data of the specimens after solution treatment. In the Tb=500 °C case, the results are good in the extrusion made with the R 12 +1° die (with a maximum error of 0.15 mm) but there is an overestimation with the R35 +3° (with a maximum error of 0.35 mm) and an underestimation in the R25 +0° and R6 -1.5° (with a maximum error of 2.5 mm). This is probably due to the lack of profile exit temperature data in the experimental trials; for this reason, it was not possible to check the accuracy of the numerical exit temperatures, that in the Tb=500 °C case are very close and sometimes higher than the annealing temperature. Moreover, these inaccuracies may also be caused by the effect of the strain rate. Using the R35 +3° die, where the bearings are longer and the material entry into the bearings zone is less sharp, the profile shows no recrystallized layer even with high ram speed. Using an R6 -1.5° die, where the bearings are non-existent (zero bearings case) and the profile has a sharp entry into the bearing zone, the profile shows the highest value of recrystallized thickness. Considering that higher bearings and choke angles correspond to a decrease in the maximum strain rate value reached during the material flow, a dependence between maximum strain rate and surface recrystallization (PCG) should be further investigated together with the effect of the profile exit temperature.
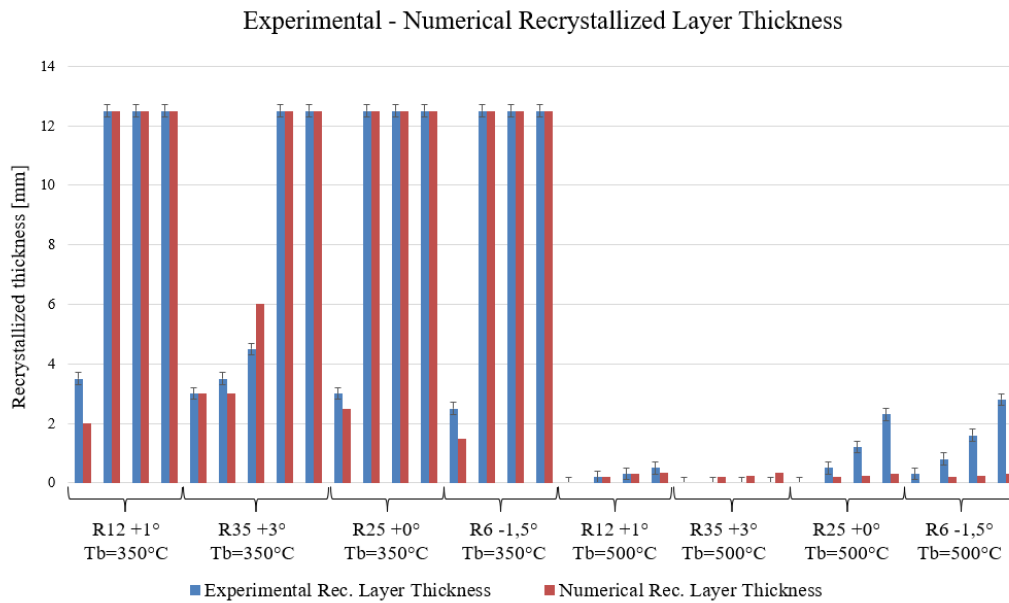
Experimental - Numerical Recrystallized Layer Thickness

Fig. 19: Comparison between experimental and numerical recrystallized layer thickness in all the investigated cases.

In Fig. 20, the assumed values of the Zener Drag pressure are reported and correlated with the exit temperatures shown in Fig. 6 for the press-quenched conditions (from 401 °C to 447 °C for the extrusions with Tb =350 °C and from 527 °C to 557 °C for the extrusions with Tb= 500 °C) and the annealing temperature of 540 °C for the solution treated conditions. The empty circles represent the Pz values assumed in the non-recrystallized specimens of the extrusions made with Tb=350 °C in the press-quenched condition, in which case it was assumed as Pz the maximum stored energy value of 1570 kJ/m^3 found in the simulation, even if it can be higher. The full green circle represents the Pz value of 819 kJ/m^3 supposed in the extrusions made with Tb=350 °C with solution treatment at 540 °C. The full orange circles represent the Pz value of 600 kJ/m^3 supposed for the extrusions made with Tb=500 °C, both for press-quenched and solution treated conditions.
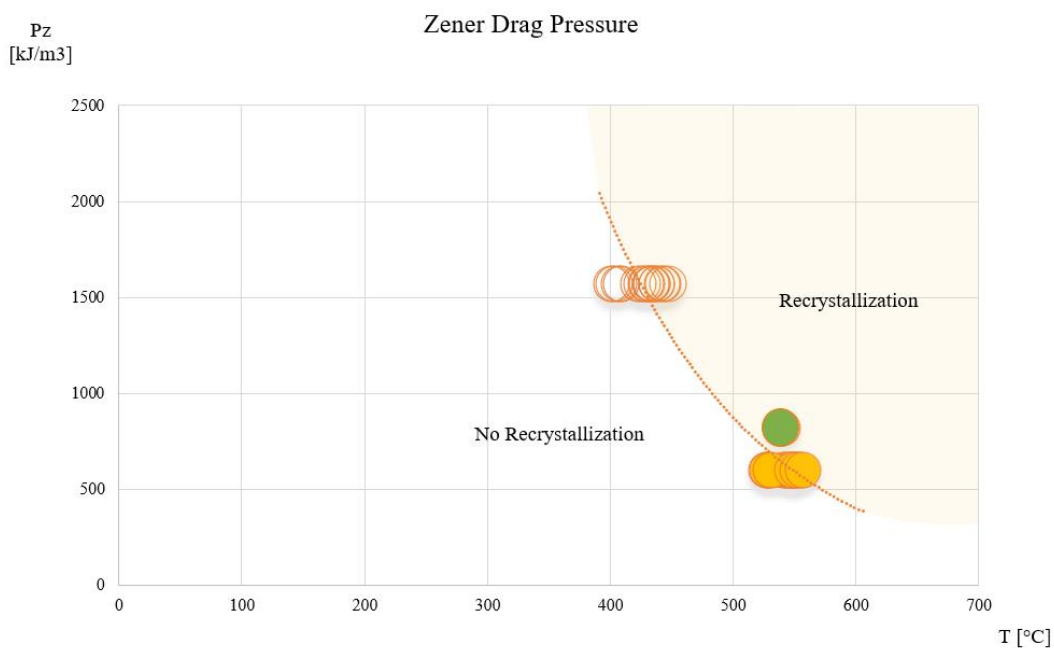

Fig. 20: Estimated Zener Drag pressures and temperatures.

The graph in Fig. 20 divides the Zener Drag pressure/Temperature area into two zones: conditions on the left side of the dashed line (which was inserted in the figure to help understand the trend of Pz in relation to the temperature) promote fibrous structures while conditions on the right side of the line recrystallized ones. It is clear the existence of a correlation between the retarding forces for recrystallization and extrusion parameters such as temperature, die geometry and ram speed that needs to be investigated and modeled through further experimental trials and research activities.

Conclusions

In the present work, the numerical modeling of the extrusion process and of the stored energy was carried out using Qform Extrusion FEM code. The experimental data were taken from the work of Parson N et al. [26], in which several industrial-scale extrusions of a AA6082 round bars were made by testing different die geometries and process conditions. The main outcomes of this work can be summarized as follows:

- The results of the various stored energy predictions of the extrusions reported in [26] were collected, compared and discussed. Consequently, by comparing the microstructures to the stored energy data, an estimation of the Zener Drag pressure was carried out. Finally, the results of the predicted recrystallized thickness were presented.

- A good correlation between numerical predictions and experimental data was found in the recrystallized thickness evaluation of the extruded profiles. The experimental data was compared to the numerical result in terms of length and shape. In the Tb=350 °C case, almost a perfect matching was found between numerical and experimental data of the specimens. One particular aspect of interest was the validation of the R35 +3° die case with ram speed of 20 mm/s and billet temperature of 350°C in the solution treated condition for which the recrystallization was correctly predicted both in the external layer and in the inner part of the round bar. In the Tb=500 °C case, the results were almost perfectly in accordance with the experimental data in the extrusions made with the R 12 +1° die, but a slightly overestimation in the R 35 +3° case and a slightly underestimation in the R25 +0° and R6 -1.5° case was observed.

- An innovative approach for the evaluation of the recrystallized thickness in the extrusion of AA6082 aluminum alloys was proposed. In order to present a complete model able to compute stored energy, Zener Drag pressure and recrystallization behaviour according to the extrusion and annealing parameters, further investigations should be carried out.

References

1. Rivas A, Muñoz P, Camero S, Quintero O (1999) Effect of the microstructure on the mechanical properties and surface finish of an extruded aa-6063 aluminum alloy. Advanced Materials Science and Technology. 2(1): 15-23.

2. Zhu H, Zhang X, Couper M, Dahle A (2009) Classification of Streaking Defects on Anodized Aluminium Extrusions. Materials Science Forum. 618-619: 349-352. https://doi.org/10.4028/www.scientific.net/MSF.618-619.349.

3. Sheppard T (2006) Prediction of structure during shaped extrusion and subsequent static recrystallisation during the solution soaking operation. Journal of Materials Processing Technology. 177: 26–35. https://doi.org/10.1016/j.jmatprotec.2006.04.099.

4. Bandar AR, Claves SR, Lu J, Matous K, Misiolek WZ, Maniatty AM (2004) Microstructural Evaluation of 6xxx Aluminum Alloys for Computer-Simulated Texture Prediction. Proceedings of the Aluminum Extrusion Technology Seminar, ET 2004, Orlando, FL, 1: 169-176.

5. Zhu R, Gong WB, Cui, H (2020) Temperature evolution, microstructure, and properties of friction stir welded ultra-thick 6082 aluminum alloy joints. Int J Adv Manuf Technol 108: 331–343. https://doi.org/10.1007/s00170-020-05422-7.

6. Parson N, Fourmann J, Beland JF (2017) Aluminum Extrusions for Automotive Crash Applications. SAE Technical Papers. 1–16. https://doi.org/10.4271/2017-01-1272.

7. Yamagata H (1995) Dynamic recrystallization and dynamic recovery in pure aluminum at 583K. Acta Metallurgica et Materialia 43(2): 723-729. https://doi.org/10.1016/0956-7151(94)00267-L

8. Gourdet S, Montheillet F (2003) A model of continuous dynamic recrystallization. Acta Materialia 51(9): 2685–2699. https://doi.org/10.1016/S1359-6454(03)00078-8.

9. McQueen HJ, Kassner ME (2004) Comments on 'a model of continuous dynamic recrystallization' proposed for aluminum. Scripta Materialia 51(5): 461–465. https://doi.org/10.1016/j.scriptamat.2004.05.027

10. McQueen HJ, Spigarelli S, Kassner ME, Evangelista E (2011) Hot Deformation and Processing of Aluminum Alloys, CRC Press, Taylor and Francis Group, Boca Raton FL, USA.

11. De Pari L, Misiolek W (2008) Theoretical predictions and experimental verification of surface, grain structure evolution for AA6061 during hot rolling. Acta Materialia 56: 6174–6185. https://doi.org/10.1016/j.actamat.2008.08.050

12. Donati L, Segatori A, El Mehtedi M, Tomesani L (2013) Grain evolution analysis and experimental validation in the extrusion of 6XXX alloys by use of a lagrangian FE code. International Journal of Plasticity. 46: 70-81. https://doi.org/10.1016/j.ijplas.2012.11.008.

13. Donati L, Dzwonczyk JS, Zhou J, Tomesani L (2008) Microstructure Prediction of Hot-Deformed Aluminium Alloys, Advances on Extrusion Technology and Simulation of Light Alloys. Stäfa, Key Engineering Materials 367: 107-116. https://doi.org/10.4028/www.scientific.net/KEM.367.107.

14. Eivani AR, Zhou J, Duszczyk J (2016) Mechanism of the formation of peripheral coarse grain structure in hot extrusion of Al-4.5Zn-1Mg. Philosophical Magazine 96(12) (2016) 1188-1196. https://doi.org/10.1080/14786435.2016.1157637.

15. Eivani AR, Zhou J, Duszczyk J (2013) Grain boundary versus particle stimulated nucleation in hot deformed Al–4.5Zn–1Mg alloy. Materials Science and Technology. 29: 517-528. https://doi.org/10.1179/1743284712Y.0000000176.

16. Furu T, Østhus R, Søreide J, Myhr O (2016) A Novel Methodology for Optimization of Properties, Costs and Sustainability of Aluminium Extrusions. Materials Science Forum. 877: 625-632. https://doi.org/10.4028/www.scientific.net/MSF.877.625.

17. Sellars CM, Zhu Q (2000) Microstructural modelling of aluminium alloys during thermomechanical processing. Materials Science and Engineering: A. 280: 1-7. https://doi.org/10.1016/S0921-5093(99)00648-6.

18. Vatne HE, Wells M (2003) Modelling of the Recrystallization Behaviour of AA5xxx Aluminum Alloys after Hot Deformation. Canadian Metallurgical Quarterly. 42: 79-88. https://doi.org/10.1179/000844303794535744.

19. Vatne HE, Furu T, Ørsund R, Nes E (1996) Modelling recrystallization after hot deformation of aluminium. Acta Materialia, 44(11): 4463-4473. https://doi.org/10.1016/1359-6454(96)00078-X.

20. Zhang C, Wang C, Zhang Q, Zhao G, Chen L, (2019). Influence of extrusion parameters on microstructure, texture, and second-phase particles in an Al-Mg-Si alloy. Journal of Materials Processing Technology. 270: 323-334. https://doi.org/10.1016/j.jmatprotec.2019.03.014.

21. Azzeddine H, Bourezg YI, Khereddine A, Baudin T, Helbert AL, Brisset F, Kawasaki M, Bradai D, Langdon T, (2019) An investigation of the stored energy and thermal stability in a Cu-Ni-Si alloy processed by high-pressure torsion. Philosophical Magazine. 100(6): 688-712. https://doi.org/10.1080/14786435.2019.1703055.

22. Eivani AR, Valipour S, Ahmed H, Zhou J, Duszczyk J (2011) Effect of the Size Distribution of Nanoscale Dispersed Particles on the Zener Drag Pressure. Metallurgical and Materials Transactions A 42: 1109–1116. https://doi.org/10.1007/s11661-010-0452-7.

23. Liu CL, Azizi H, Parson N, Poole W, Du Q (2017) Microstructure evolution during homogenization of Al-Mg-Si-Mn-Fe alloys: Modelling and experimental results. Transactions of Nonferrous Metals Society of China. 27: 747-753. https://doi.org/10.1016/S1003-6326(17)60085-2.

24. Gandin CA, Jacot A (2007) Modeling of precipitate-free zone formed upon homogenization in a multi-component alloy. Acta Materialia. 55: 2539-2553. https://doi.org/10.1016/j.actamat.2006.11.047.

25. Cai M, Robson J, Lorimer GW (2007) Simulation and control of dispersoids and dispersoid-free zones during homogenizing an AlMgSi alloy. Scripta Materialia 57(7) (2007) 603-606. https://doi.org/10.1016/j.scriptamat.2007.06.008.

26. Parson N, Maltais A, Jowett C (2012) The Influence of Die Bearing Geometry on Surface Recrystallisation of 6xxx Extrusions. Proceedings of the Tenth International Aluminum Extrusion Technology Seminar ET 2012, 1: 19-32.

27. Van Geertruyden WH, Misiolek WZ, Wang PT (2005) Evolution of surface recrystallization during indirect extrusion of 6xxx aluminum alloys. Metall. Mater. Trans. 36: 1049–1056. https://doi.org/10.1007/s11661-005-0298-6.

28. Furu T, Shercliff HR, Baxter GJ, Sellars CM (1999) The influence of transient deformation conditions on recrystallization during thermomechanical processing of an Al–1% Mg alloy, Acta Materialia 47(8): 2377-2389. https://doi.org/10.1016/S1359-6454(99)00113-5.

29. Xu J, Xu W, Li J, Zeng X, Li K, Shan D (2021) Preform design and microstructure-property analysis for isothermal extrusion of complex box-shaped components. Int J Adv Manuf Technol 114: 2339–2356. https://doi.org/10.1007/s00170-021-07030-5

30. Giarmas E, Tzetzis D (2022) Optimization of die design for extrusion of 6xxx series aluminum alloys through finite element analysis: a critical review. Int J Adv Manuf Technol 119: 5529–5551. https://doi.org/10.1007/s00170-022-08694-3.

31. Mahmoodkhani Y, Chen J, Wells M, Poole W, Parson N (2019) The Effect of Die Bearing Geometry on Surface Recrystallization During Extrusion of an Al-Mg-Si-Mn Alloy. Metallurgical and Materials Transactions A 50: 1-12. https://doi.org/10.1007/s11661-019-05437-0.

32. Liu Y, Xu J, Zhang Z, Liu G, Shan D, Zhang L, Guo B (2022) Micro-extrusion process and microstructure evolution of miniature heat pipe in 6063 aluminum alloy. Int J Adv Manuf Technol 120: 6463–6480. https://doi.org/10.1007/s00170-022-09096-1.

33. Ji H, Nie H, Chen W, Ruan X, Pan P, Zhang J (2017) Optimization of the extrusion die and microstructure analysis for a hollow aluminum alloy profile. Int J Adv Manuf Technol 93: 3461–3471. https://doi.org/10.1007/s00170-017-0720-4.

34. Gamin Y, Akopyan T, Koshmin A, Dolbachev A, Aleshchenko A, Galkin SP, Romantsev BA (2020) Investigation of the microstructure evolution and properties of A1050 aluminum alloy during radial-shear rolling using FEM analysis. Int J Adv Manuf Technol 108: 695–704. https://doi.org/10.1007/s00170-020-05227-8.

35. Zhang C, Zhao G, Chen H, Guan Y, Kou F (2012) Numerical simulation and metal flow analysis of hot extrusion process for a complex hollow aluminum profile. Int J Adv Manuf Technol 60: 101–110 (2012). https://doi.org/10.1007/s00170-011-3609-7.

36. Rios P, Siciliano F, Sandim H, Lesley R, Padilha A (2005) Nucleation and growth during recrystallization. Materials Research 8(3): 225-238 https://doi.org/10.1590/S1516-14392005000300002.

37. Zhu Q, Abbod MF, Talamantes-Silva J, Sellars CM, Linkens DA, Beynon JH (2003) Hybrid modeling of aluminium-magnesium alloys during thermomechanical processing in terms of physically-based, neuro-fuzzy and finite elements models. Acta Materialia 51: 5051-5062. https://doi.org/10.1016/S1359-6454(03)00353-7.

38. Schindler I, Kawulok P, Ocenasek V, Opěla P, Kawulok R, Rusz S (2019) Flow Stress and Hot Deformation Activation Energy of 6082 Aluminium Alloy Influenced by Initial Structural State. Metals 9: 1248-1263. https://doi.org/10.3390/met9121248.

39. Negozio M, Pelaccia R, Donati L, Reggiani B, Pinter T, Tomesani L (2021) Finite Element Model Prediction of Charge Weld Behaviour in AA6082 and AA6063 Extruded Profiles. Journal of Materials Engineering and Performance, 30: 4691-4699. https://doi.org/10.1007/s11665-021-05752x

40. Negozio M, Pelaccia R, Donati L, Reggiani B (2022) FEM Analysis of the Skin Contamination Behavior in the Extrusion of a AA6082 Profile. Key Engineering Materials 926: 452-459. https://doi.org/10.4028/p-y37nm3

41. Bandini C, Reggiani B, Donati L, Tomesani L (2015) Code Validation and Development of User Routines for Microstructural Prediction with Qform. Materials Today: Proceedings 2(10): 4904-4914. https://doi.org/10.1016/j.matpr.2015.10.052

42. -Reggiani, B, Donati, L, Tomesani, L (2017) ICEB - international conference on extrusion and benchmark. Light Metal Age, 75(5): 52-60.

43. Hensel A, Spittel T (1978) Kraft und Arbeitsbedarf bildsamer Formgeburgsverfahren, 1. Auflage, Leipzig: VEB Deutscher Verlag fur Grundstoffindustrie.
44. Negozio M, Pelaccia R, Donati L, Reggiani B, Pinter T, Tomesani L (2021) Finite Element Model Prediction of Charge Weld Behaviour in AA6082 and AA6063 Extruded Profiles. Journal of Materials Engineering and Performance 30: 4691–4699. https://doi.org/10.1007/s11665-021-05752-x.